Developmental Biology 438 (2018) 33–43

Contents lists available at ScienceDirect

Developmental Biology

journal homepage: www.elsevier.com/locate/developmentalbiology

Protein tyrosine kinase 7 regulates extracellular matrix integrity and mesenchymal intracellular RAC1 and myosin II activities during Wolffian duct morphogenesis

Bingfang Xu[a], Sérgio A.A. Santos[b], Barry T. Hinton[a,*]

[a] Department of Cell Biology, University of Virginia Health System, PO Box 800732, Charlottesville, VA 22908, USA
[b] Institute of Biosciences, São Paulo State University (UNESP), Botucatu, Brazil

ARTICLE INFO

Keywords:
PTK7
RAC1
Myosin II
ECM
Wolffian duct
Morphogenesis
Mesenchyme

ABSTRACT

Wolffian duct morphogenesis must be highly coordinated with its specialized function of providing an optimal microenvironment for sperm maturation. Without normal Wolffian duct morphogenesis, male infertility will result. Our previous study showed that mediolateral and radial intercalation of epithelial and mesenchymal cells respectively, were major drivers of ductal elongation and were regulated by protein tyrosine kinase 7 (PTK7), a member of the planar cell polarity (PCP) non-canonical Wnt pathway. To understand the mechanism by which PTK7 regulates cell rearrangement/intercalation, we investigated the integrity of the extracellular matrix (ECM) and the activity of intracellular cytoskeleton mediators following loss of *Ptk7*. Abnormal assembly of nephronectin, laminin, and collagen IV at the basement membrane and fibrosis-like deposition of fibrilla collagen in the interstitium were observed in *Ptk7* knockout Wolffian ducts. Further, the activity levels of RAC1 and myosin II, two cytoskeleton mediators, decreased in the *Ptk7* knockout mesenchyme compared to controls. In addition, *in-vitro* experiments suggested that alterations of ECM and cytoskeleton mediators resulted in changes in Wolffian duct morphogenesis. When *in-vitro*-cultured Wolffian ducts were treated with collagenase IV, the degree of cross-linked fibrilla collagen was reduced, Wolffian duct elongation and coiling were significantly reduced, and an expanded cyst-like duct was observed. When Wolffian ducts were treated with RAC1 inhibitor NSC23766, mesenchymal fibrilla collagen was disassembled, and Wolffian duct elongation was significantly reduced. Our findings provide evidence that PTK7 regulates ECM integrity and the activity levels of RAC1 and myosin II, which in turn regulates Wolffian duct morphogenesis and therefore, epididymal function.

1. Introduction

It is very clear that the epididymis plays a crucial role in the maturation of spermatozoa, and without a fully developed and functional epididymis, male infertility will result. It is especially important to understand the mechanisms that regulate the development of the epididymis because disruptions to epididymal function often arise as a consequence of abnormal development (Girgis et al., 1969; Hinton et al., 2011; Kroovand and Perlmutter, 1981; Turek et al., 1994).

The epididymis develops from anterior part of the Wolffian duct. Elongation and coiling of the Wolffian/epididymal duct are not trivial events and must be highly coordinated with its specialized function of providing a unique luminal fluid microenvironment for sperm maturation (Hinton et al., 2011). Remarkably, the adult mouse epididymal duct is 1.2 m, whereas the human epididymal is 6 m long (Hinton et al., 2011; Joseph et al., 2009).

Examining the role of protein tyrosine kinase 7 (*Ptk7*) using brachyury (T; mesoderm) (Perantoni et al., 2005) conditional Cre knockout (designated *Ptk7* TCre-cKO) mice uncovered a series of unique mechanisms by which the Wolffian duct elongates (Xu et al., 2016). Briefly, (i) Epithelial cells divided in a random orientation relative to the elongation axis of the duct. (ii) Mediolateral cell rearrangements/intercalation of epithelial cells was required to elongate the duct while maintaining a relatively unchanged duct diameter. (iii) Normal epithelial cells were planar polarized, which was characterized by oriented cell elongation, oriented cell rearrangements, and polarized activity of regulatory light chain myosin II; the epithelium of *Ptk7* TCre-cKO Wolffian ducts was not planar polarized. Loss of *Ptk7* resulted in a duct that had failed to undergo elongation, which subsequently resulted in a shortened adult epididymis with failure of sperm to develop motility.

Our previous studies also suggested that mediolateral intercalation

* Corresponding author.
E-mail address: bth7c@virginia.edu (B.T. Hinton).

https://doi.org/10.1016/j.ydbio.2018.03.011
Received 15 January 2018; Received in revised form 21 February 2018; Accepted 13 March 2018
Available online 23 March 2018
0012-1606/

of epithelial cells was coordinated with radial intercalation of smooth muscle/mesenchymal cells (SMM) surrounding the epithelial duct (Xu et al., 2016) together with the collective en masse movement of interstitial mesenchymal cells. During normal Wolffian duct morphogenesis, SMM cells surrounding the epithelial duct become elongated and have reduced layers of cells. The change in shape and organization of SMM cells suggested a process of radial intercalation. Radial intercalation differs from epithelial mediolateral intercalation in that during radial intercalation, cells move in between layers and across the tissue perpendicular to the surface, thereby thinning that layer of cells and increasing its surface area (Walck-Shannon and Hardin, 2014). In contrast to controls, SMM cells from *Ptk7* TCre-cKO ducts were wider, random shaped, disorganized and comprised several layers surrounding the duct, suggesting a defect in radial intercalation (Xu et al., 2016).

Deletion of *Ptk7* from the epithelium and mesenchyme resulted in the strong defective phenotype. However, deletion of *Ptk7* from the epithelium alone or deletion of *Ptk7* from SMM cells alone resulted in much milder phenotypes compared to the phenotype observed in animals with deletion of *Ptk7* from both tissues (Xu et al., 2016). This finding suggests that mediolateral intercalation of epithelial cells is coordinated with radial intercalation of SMM cells and together they play an important role in Wolffian duct morphogenesis, and PTK7 regulates both types of cell rearrangements.

Cell rearrangements during morphogenesis requires a combination of mechanisms (Walck-Shannon and Hardin, 2014), for example, extracellular matrix remodeling and intracellular cytoskeletal events exert forces that are needed for cell rearrangements (Bonnans et al., 2014; Clause and Barker, 2013; Sit and Manser, 2011; Vicente-Manzanares et al., 2009; Walck-Shannon and Hardin, 2014) Therefore, we tested the hypothesis that PTK7 regulated the integrity of the components of the ECM and regulators of the intercellular cytoskeleton during Wolffian duct morphogenesis. Our strategy and approaches to test this hypothesis were several folds: (1) to examine the regulation of ECM genes by *Ptk7* using RNAseq. Our goal was to specifically focus on ECM genes using an approach that would provide reliable and consistent data. (2) To focus on a small number of ECM components that are well documented to play a role in ECM function, and use a number of imaging approaches to detect changes in the integrity of those ECM components following loss of *Ptk7*. (3) To examine the role of intracellular cytoskeleton regulators, myosin II and Rho GTPases during Wolffian duct morphogenesis and their regulation by PTK7.

2. Results

2.1. Differentially expressed ECM genes in TCre-cKO Wolffian ducts compared to controls

An RNASeq approach was used to identify and quantify genes that were regulated by *Ptk7*. The RNAseq analysis of mRNA expression in Wolffian ducts of control and TCre-cKO E18.5 embryos identified 183 differentially expressed genes (adjusted p value < 0.05). Examining the differentially expressed genes using Gene Ontology (GO) and Ingenuity Pathway Analysis (IPA) identified that the Wnt signaling pathway was over-representative of the signaling pathway and ECM components and plasma membrane components as two groups of over-representative of cellular components. Our study then focused on ECM components because of their well-documented roles in the regulation of cell rearrangements. Table 1 lists significantly differentially expressed ECM genes. From this group, the following genes had higher numbers of transcripts (baseMean > 1000): adhesion G protein-coupled receptor G1 (*Adgrg1*), embigen (*Emb*), wingless-type MMTV integration site family member 4 (*Wnt4*), insulin-like growth factor binding protein 5 (*Igfp5*), nephronectin (*Npnt*), spondin2 (*Spon2*), transforming growth factor beta induced (*Tgfbi*), and epidermal growth factor-like protein 6 (*Egfl6*). Of which *Adgrg1, Emb, Npnt, and Egfl6* were down-regulated, and *Wnt4, Igfp5, Spon2, and Tgfbi* were up-regulated in TCre-cKO Wolffian ducts compared to controls.

Table 1
Differentially expressed ECM genes in TCre-cKO Wolffian ducts compared to controls.

Symbol	Description	BaseMean	log2FoldChange	padj
Olfml2b	olfactomedin-like 2B	432	0.501	0.000437
Gpc5	glypican 5	119	−0.651	0.000568
Adgrg1	adhesion G protein-coupled receptor G1	2640	−0.502	0.00206
Emb	embigin	1210	−0.43	0.00211
Wnt4	wingless-type MMTV integration site family, member 4	1770	0.427	0.00243
Igfbp5	insulin-like growth factor binding protein 5	38800	0.377	0.00399
Npnt	nephronectin	3690	−0.378	0.0107
Itgb6	integrin beta 6	46.7	−0.534	0.0141
Spon2	spondin 2, extracellular matrix protein	1420	0.407	0.016
Tgfbi	transforming growth factor, beta induced	5130	0.378	0.0223
Egfl6	EGF-like-domain, multiple 6	4790	−0.34	0.0326
Gm4980	predicted gene 4980	68.5	0.476	0.0378
Wnt7b	wingless-type MMTV integration site family, member 7B	634	−0.406	0.049

Note: the list order is based on the adjusted p value (padj).

2.2. Localization of NPNT in epithelial basement membrane and capsule of TCre-cKO and control Wolffian ducts

Among differentially expressed ECM genes (Table 1), NPNT was selected for further studies because of its importance in ECM organization and kidney morphogenesis (Linton et al., 2007). NPNT was localized to the epithelial basement membrane and the capsule surrounding the Wolffian duct (Fig. 1A-D, yellow and light blue arrows, respectively). Confocal cross section images and whole mount immunofluorescence and 3D reconstruction of a portion of Wolffian ducts showed that NPNT protein was highly expressed but disorganized in the basement membrane in E18.5 TCre-cKO mice (Fig. 1B and D, yellow arrows). In contrast, the control duct showed diffuse NPNT labelling at the basement membrane (Fig. 1A and C, yellow arrows). Movies of 3D reconstruction of NPNT whole mount immunofluorescence from controls and cKOs were generated and shown as supplementary movies 1 and 2.

Supplementary material related to this article can be found online at http://dx.doi.org/10.1016/j.ydbio.2018.03.011.

Our NPNT data suggested that PTK7 regulated ECM components at the expression and protein deposition level. Therefore, the next series of experiments focused on the localization of another two ECM proteins of known function: (1) Laminin, which is a major component of the basement membrane. (2) Collagen IV (COL4), which is a major component of the basement membrane and is a component of the capsule surrounding the Wolffian duct, and is an ECM component of mesenchymal cells.

2.3. Localization of laminin in epithelial and endothelial basement membranes and capsule of TCre-cKO and control Wolffian ducts

Laminin was localized to the epithelial and endothelial basement membranes (Fig. 1C and D, yellow and magenta arrows, respectively), and the capsule surrounding the Wolffian duct (Fig. 1C and D, light blue arrows). Confocal images of TCre-cKO Wolffian ducts showed that laminin formed bundles of fibers at the basement membrane (Fig. 1D, yellow arrow) compared to a diffuse localization in controls (Fig. 1C, yellow arrow).

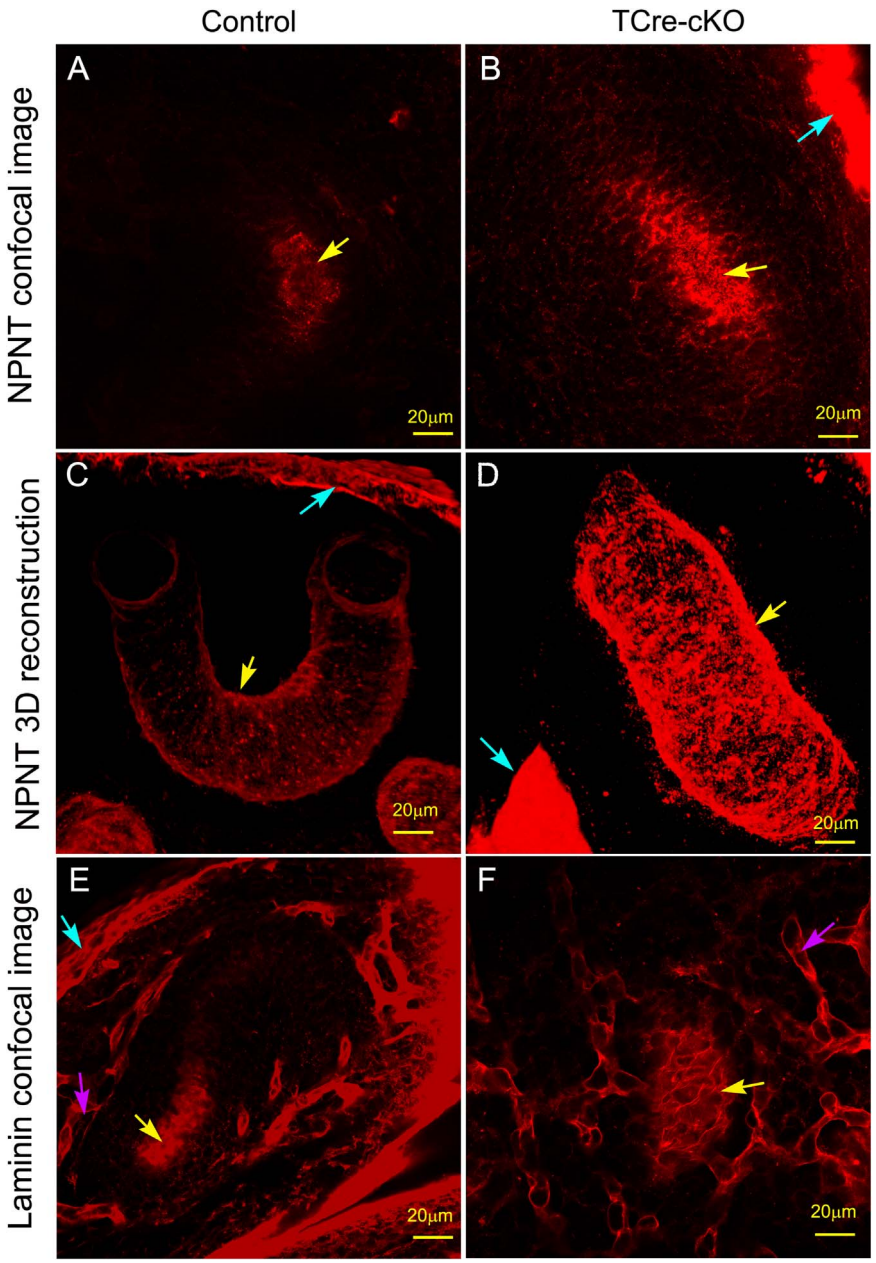

Fig. 1. Localization of NPNT and Laminin in E18.5 Wolffian ducts. (A) Representative confocal image of NPNT within the basement membrane of control E18.5 Wolffian ducts. (B) Representative confocal image of NPNT within the basement membrane of TCre-cKO E18.5 Wolffian ducts. (C) 3D reconstruction image of NPNT in control E18.5 Wolffian ducts. (D) 3D reconstruction image of NPNT in TCre-cKO E18.5 Wolffian ducts. Note the abundance and disorganization of NPNT within the basement membrane of TCre-cKOs. (E) Representative confocal image of laminin within the basement membrane of control E18.5 Wolffian ducts. (F) Representative confocal image of laminin within the basement membrane of TCre-cKO E18.5 Wolffian ducts. Note the diffuse localization pattern of laminin within the basement membrane of E18.5 control Wolffian ducts and laminin-labeled fiber bundles within the basement membrane of TCre-cKOs. Yellow arrows show the basement membrane of the epithelial ducts. Magenta arrows show the basement membrane of endothelial ducts. Light blue arrows show the capsule of the Wolffian duct. (For interpretation of the references to color in this figure legend, the reader is referred to the web version of this article.)

2.4. Localization of COL4 in epithelial and endothelial basement membranes, ECM of the mesenchyme, and capsule of TCre-cKO and control Wolffian ducts

COL4 was abundant within the basement membrane of epithelial and endothelial ducts (Fig. 2, yellow and magenta arrows, respectively), the capsule of the Wolffian duct (Fig. 2, light blue arrow), and was present throughout the ECM of SMM and interstitial/mesenchymal (ISM) cells (Fig. 2, white arrows and asterisk, respectively).

An increase in COL4 immunofluorescence was observed within the epithelial basement membrane and the ECM of SMM and ISM cells in TCre-cKOs compared to controls (Fig. 2A and B, yellow, white arrows and asterisks, respectively).

Confocal images of the surface of the basement membrane revealed that COL4 had abnormal aggregation at the basement membrane in TCre-cKOs compared to diffuse localization in controls (Fig. 2C and D, arrowheads).

Second harmonic generation imaging showed that fibrilla collagen had a low intensity at the basement membrane of the epithelium and in the ECM of SMM cells but was abundant in the ECM of ISM cells (Fig. 2E and F, yellow and white arrows, and asterisks, respectively). The mean fibrilla collagen intensity in ISM of TCre-KO was 51.6 ± 8.0 (mean ± SEM) compared to 31.4 ± 3.1 in controls. Intensive signals from fibrosis-like deposition were observed within TCre-cKO ISM area (Fig. 2F, double arrowheads) but not in controls.

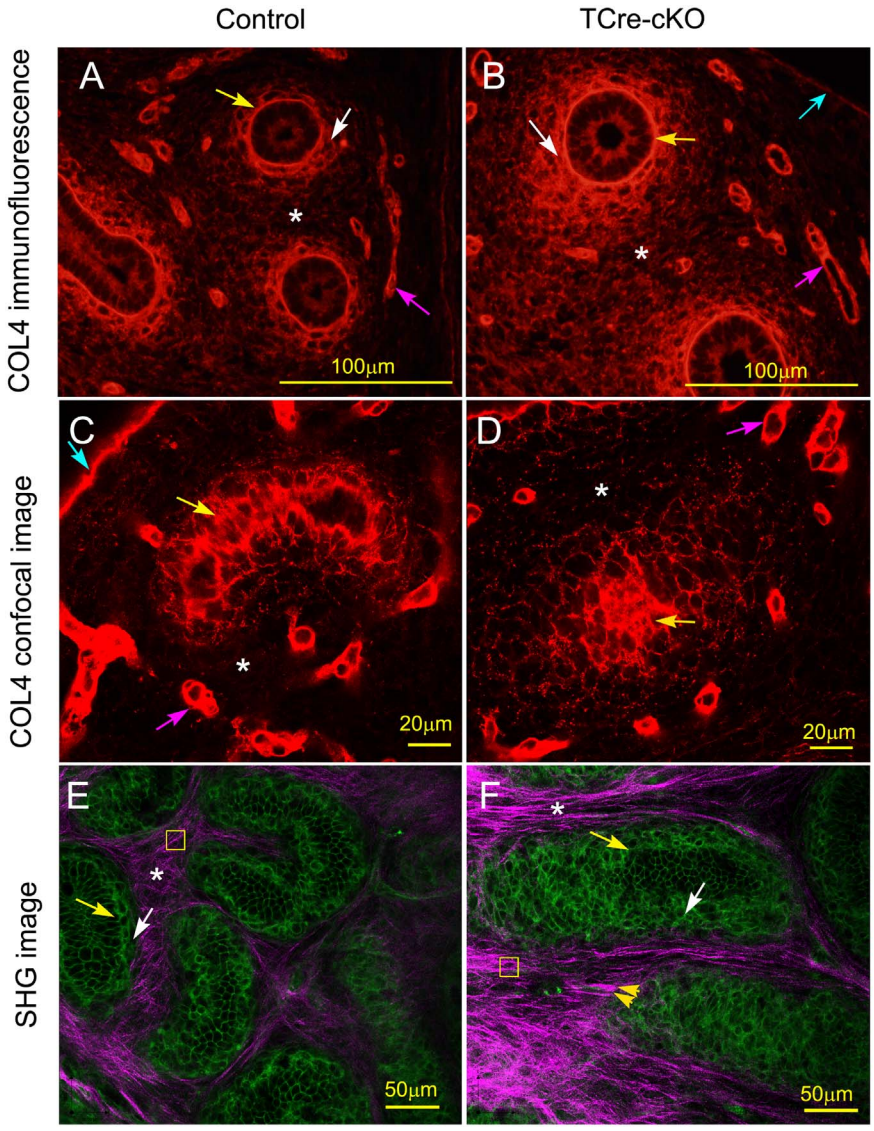

Fig. 2. Localization of COL4 in E18.5 control and TCre-cKO Wolffian ducts. (A-B) Immunofluorescence images of COL4 in tissue sections of control and TCre-cKO Wolffian ducts, respectively. (C-D) Confocal images of COL4 at the surface of the epithelial basement membrane of control and TCre-cKO Wolffian ducts, respectively. (E-F) Fibrilla collagen (purple) in the mesenchyme of control and TCre-cKO Wolffian ducts, respectively. EGFP (green) labels the cell membrane of all Wolffian duct cells. Note the increase in fibrilla collagen content within the interstitial area of the TCre-cKO Wolffian duct compared to control. Double arrowheads show fibrosis-like deposition of collagen. Yellow arrows show the basement membrane of the epithelial ducts. White arrows show the SMM. Asterisks show the ISM. Magenta arrows show the basement membrane of endothelial ducts. Light blue arrows show the capsule of the Wolffian duct. Yellow squares represent the area that was selected in the ISM to measure signal intensity. (For interpretation of the references to color in this figure legend, the reader is referred to the web version of this article.)

2.5. The role of collagen during Wolffian duct elongation and coiling

To examine the role of collagen during Wolffian duct morphogenesis, an *in vitro* approach was employed, in which E15.5 ducts were exposed to 0.1 mg/ml collagenase IV for 1, 5 or 10 min. The 5 or 10 min of exposure to a low concentration of collagenase IV resulted in a decrease in Wolffian duct elongation and coiling (Fig. 3A and B). Notably, cyst-like dilatation and expansion in multiple spots along the Wolffian duct were observed over 48–72 h of culture (Fig. 3A and B, arrow) in the 5-min-treatment group, and fewer but larger expansions were observed in the10-minute-treatment group. Expansion was not observed in control and 1-min-treatment groups (Fig. 3B).

The integrity of fibrilla collagen was examined using second harmonic generation imaging following treatment of collagenase IV for 5 min and then cultured for 24 h. As shown in Fig. 3C, the amount of cross-linked collagen fibrils within the interstitium was reduced following collagenase treatment. The number of points joined between fibers (Fig. 3C, asterisks in the inserts) was significantly higher in controls (23 ± 1, arbitrary unit, mean ± SEM) compared to TCre-KOs (8 ± 1.2).

In the next series of experiments we focused on examining the regulation RAC1 and myosin II, key intracellular cytoskeleton regulators, by PTK7.

2.6. Differential activities of RAC1 and myosin II in TCre-cKO and control mesenchymal cells

RAC1 activity was determined by immunolabeling using an antibody against GTP-bound RAC1 to the plasma membrane. Active RAC1 was not present in epithelial cells but was localized to the cell membrane of mesenchymal cells (Fig. 4A and D). Representative images and plot profiles of the lines across the mesenchyme (Fig. 4A, A′, D and D′) showed that the labelling intensity of active RAC1 was higher in ISM cells (Fig. 4, magenta arrow) compared to SMM cells

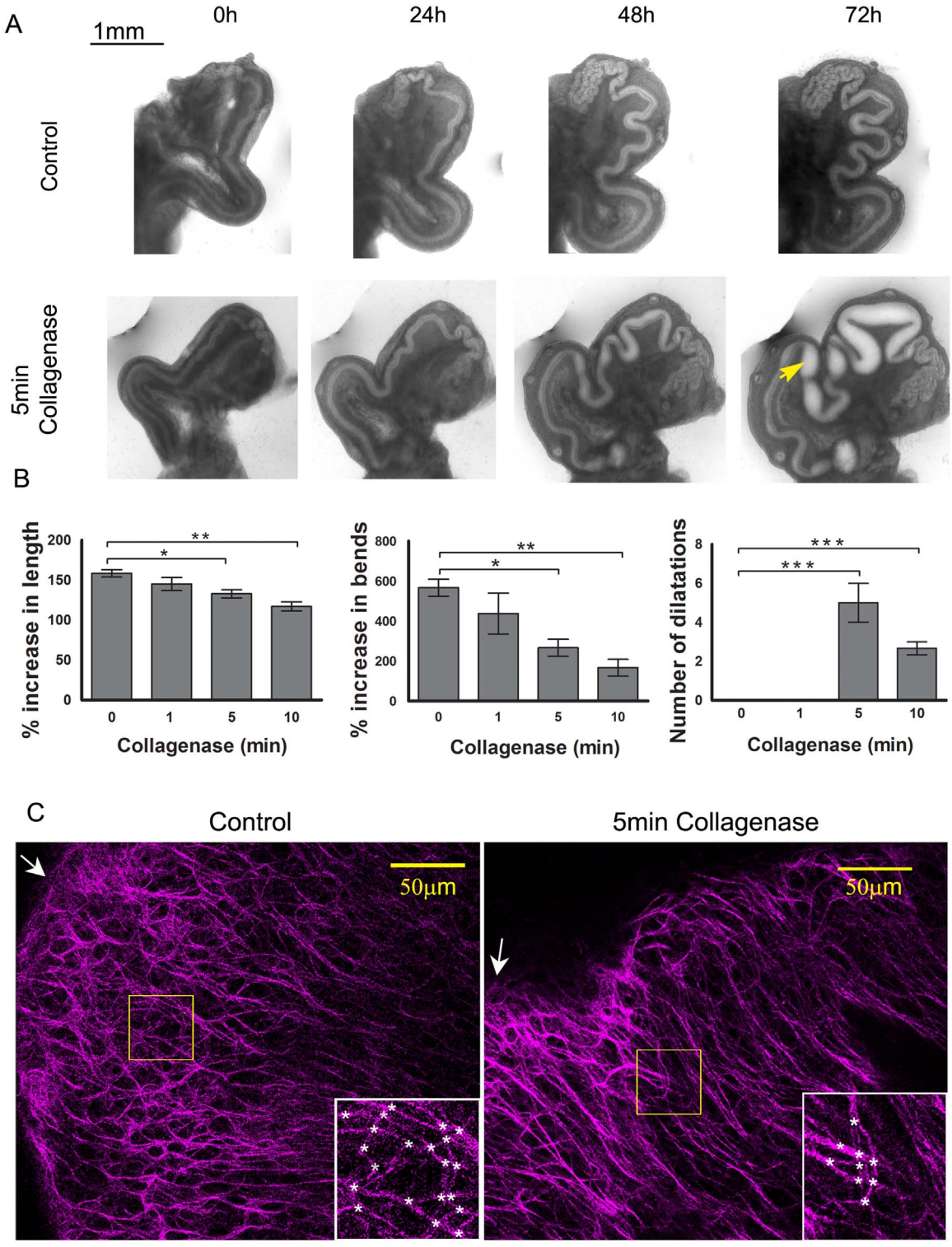

Fig. 3. The effect of collagenase IV treatment during *in vitro* Wolffian duct culture. (A) Wolffian ducts treated without (control) or with collagenase IV (0.1 mg/ml) for 5 min. Yellow arrow shows a small region of ductal expansion. (B) The effect of collagenase IV treatment on Wolffian duct elongation, coiling and duct dilatation. Data are represented as mean ± SEM, n ≥ 3. (C) Representative images from second harmonic generation imaging that identifies fibrilla collagen within the ISM of control Wolffian ducts (left panel) and from Wolffian ducts incubated with collagenase for 5 min and then cultured for 24 h (right panel). The images are cross sections of the subcapsular layer, which is 10 μm below the capsule surface. White arrows show the edge of the capsule. The inserts are the enlarged areas marked by the yellow squares, the asterisks show the points joined between fibers. (For interpretation of the references to color in this figure legend, the reader is referred to the web version of this article.)

(Fig. 4, yellow arrow). Measurement of the labelling intensity of multiple areas (Fig. 4A and D, yellow squares) showed that RAC1 activity decreased in SMM and ISM of TCre-cKOs compared to controls (Fig. 4G). Notably, the thickness of SMM in TCre-cKOs increased significantly compared to controls (Fig. 4G).

Myosin II activity was determined by immunolabelling using an antibody against phosphorylated regulatory light chain, pRLC, of myosin II. pRLC was localized to the cell membrane of epithelial and mesenchymal cells (Fig. 4B and E). A higher level of labelling intensity of pRLC was observed in SMM cells compared to ISM cells (Fig. 4B, B′,

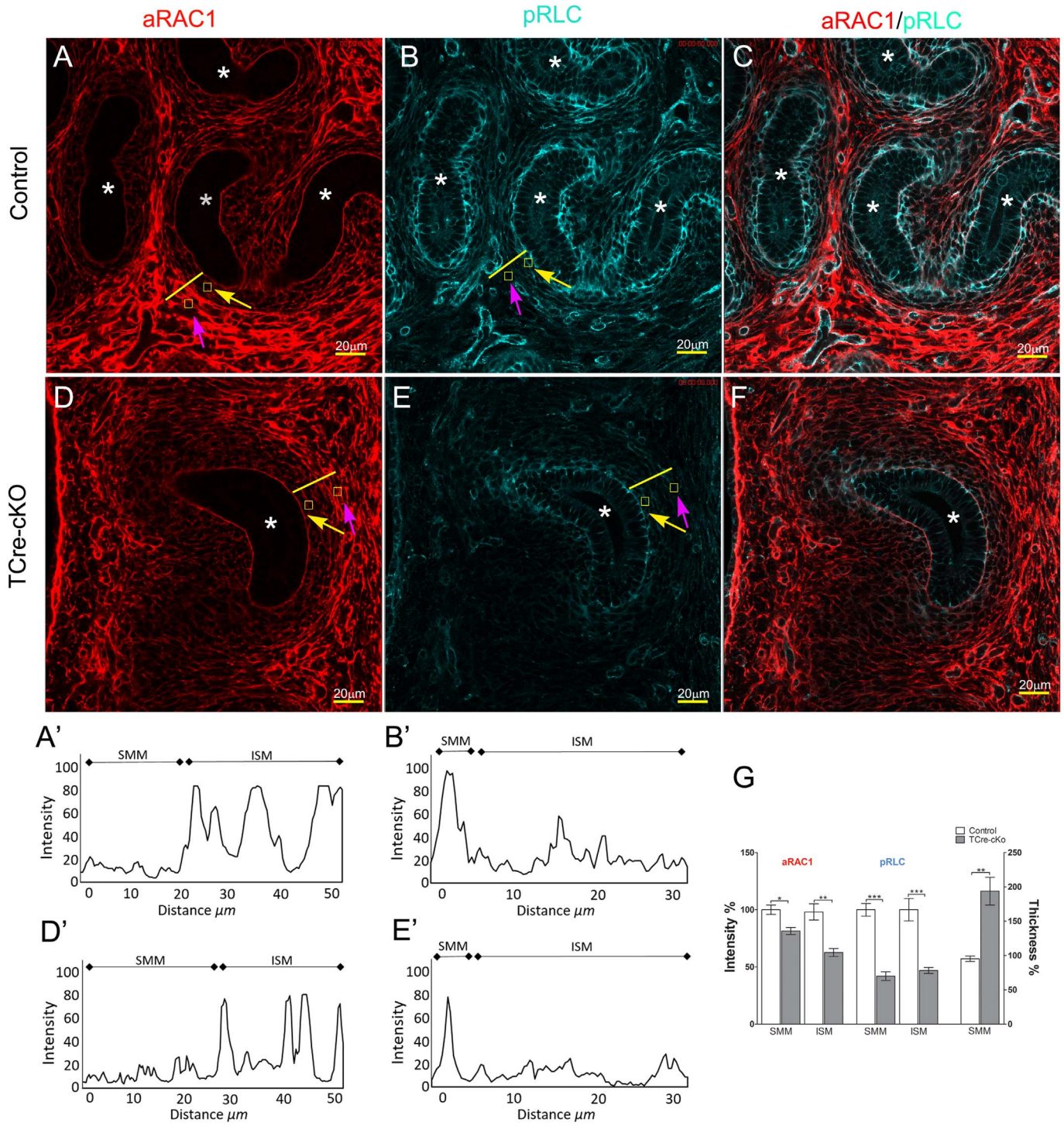

Fig. 4. Immunolocalization of active RAC1 (aRAC1) and pRLC in E18.5 control and TCre-cKO Wolffian ducts. (A-C) Confocal images of active RAC1 (red), pRLC (cyan), and the merged image in control Wolffian ducts. (D-F) Confocal images of active RAC1 (red), pRLC (cyan), and the merged image in TCre-cKOs Wolffian ducts. (A′and D′) Plot profiles of the lines in A and D showing labelling intensity of active RAC1 in SMM and ISM of controls and TCre-cKOs. (H) Plot profiles of the lines in B and E showing labelling intensity of pRLC in SMM and ISM of controls and TCre-cKOs. (G) Measurement of label intensity of active RAC1 and pRLC in the SMM and ISM in both controls and TCre-cKOs and measurement of thickness of SMM in controls and TCre-cKOs. Yellow squares represent the areas that were selected in SMM and ISM to measure labelling intensity. Yellow arrows label SMM, magenta arrows label ISM, and asterisks label the epithelium. Data are represented as mean ± SEM, n ≥ 3. (For interpretation of the references to color in this figure legend, the reader is referred to the web version of this article.)

E and E′). The labelling intensity of pRLC in SMM and ISM cells was reduced following loss of *Ptk7* (Fig. 4G).

Active RAC1 and pRLC localization did not overlap with a higher activity level of pRLC in epithelial and SMM cells but a higher activity level of active RAC1 in ISM and capsule (Fig. 4C and F).

Active RAC1 was co-localized with membrane-tagged EGFP in SMM cells (Fig. 5A), confirming its membrane localization. Loss of *Ptk7* did not change the membrane localization of active RAC1 (Fig. 5B). 3D reconstruction of active RAC1 labelling, which was also illustrated by surface plot of an area in SMM, showed that active RAC1 oriented perpendicular to the duct elongation axis in controls but not in TCre-cKOs (Fig. 5C, D, C′ and D′).

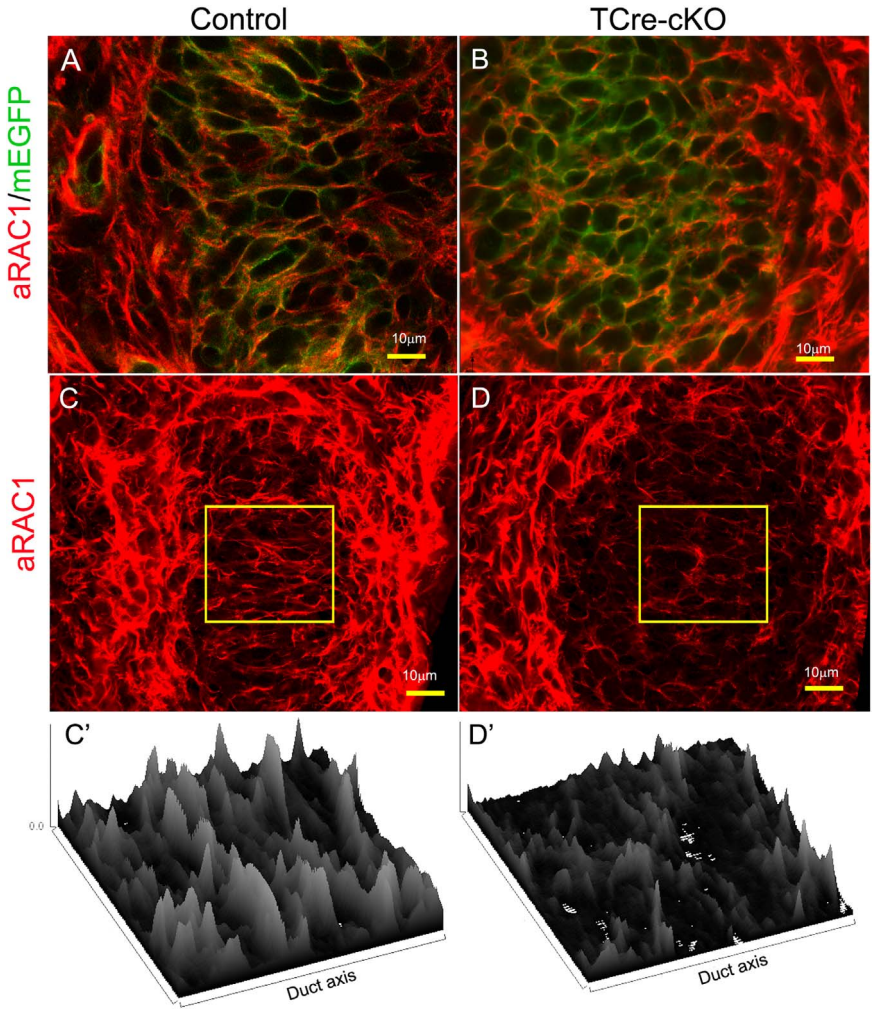

Fig. 5. Immunolocalization of active RAC1 (aRAC1) in the Wolffian duct SMM of E18.5 controls and TCre-cKOs. (A-B) Co-localization of active RAC1 (red) with membrane EGFP (green) in SMM cells of controls and TCre-cKOs. Cell membranes of all epididymal cells are green because the mouse line carries a floxed mTmG cassette. (C-D) 3D reconstruction images of active RAC1 in SMM cells of controls and TCre-cKOs. (C′-D′) Corresponding surface plots of the selected areas in C and D showing bundles of RAC1-GTP positive fiber orients perpendicularly towards the duct elongation axis in control SMM cells but not in TCre-cKOs. (For interpretation of the references to color in this figure legend, the reader is referred to the web version of this article.)

2.7. The roles of RAC1 in ECM assembly and Wolffian duct elongation

E15.5 Wolffian ducts were incubated with NSC23766, an inhibitor of RAC1 activity for up to 48 h. To show the drug was reversible, the drug was removed after 48 h, and the ducts were incubated for a further 24 h (Fig. 6A). Inhibition of RAC1 activity did not prevent the Wolffian ducts from increasing their bend number during *in vitro* culture (Fig. 6B). However, inhibition of RAC1 activity resulted in a decrease in length between bends, which subsequently resulted in a decrease in total length of the Wolffian duct (Fig. 6B).

Wolffian duct controls and those incubated with the inhibitor for 24 h were subjected to morphological analysis using H and E staining. In controls, mesenchymal cells were tightly packed surrounding the epithelial duct, whereas mesenchymal cells in the treatment group were scattered within the interstitium (Fig. 6C).

Wolffian duct controls and those incubated with the inhibitor for 24 h were analyzed for fibrilla collagen using second harmonic generation imaging. As shown in Fig. 6C, inhibition of RAC1 activity resulted in loss of organization/assembly of collagen compared to control Wolffian ducts.

3. Discussion

It is clear that PTK7 regulates Wolffian duct morphogenesis, but the underlying molecular and cellular mechanisms are unclear. Studies on other model systems revealed that the combined effort of ECM remodeling and intracellular cytoskeletal events generates forces that are needed for cell rearrangements during morphogenesis (Bonnans et al., 2014; Clause and Barker, 2013; Sit and Manser, 2011; Vicente-Manzanares et al., 2009; Walck-Shannon and Hardin, 2014). Therefore, we hypothesized that PTK7 was involved in regulation of ECM and intracellular signaling and proposed a mechanism, of which PTK7 regulates both aspects (Fig. 7).

3.1. PTK7 regulates ECM

The first clue that the ECM was playing a role during Wolffian duct morphogenesis was from our published microarray study (Snyder et al., 2010). Changes in gene expression of a number of ECM components were observed in different regions: efferent ducts, epididymis, and vas deferens, and at different time points (E14.5-P1). In the current study, RNAseq analysis revealed that PTK7, an important mediator of Wolffian duct morphogenesis (Xu et al., 2016), regulated mRNA expression of multiple ECM genes. Furthermore, whole mount immunofluorescence showed that PTK7 also regulated ECM components such as NPNT, laminin, COL4 at the deposition and organization levels.

It is well known that morphogenesis requires constant remodeling of the ECM (Bonnans et al., 2014). Presumably, the alteration of the

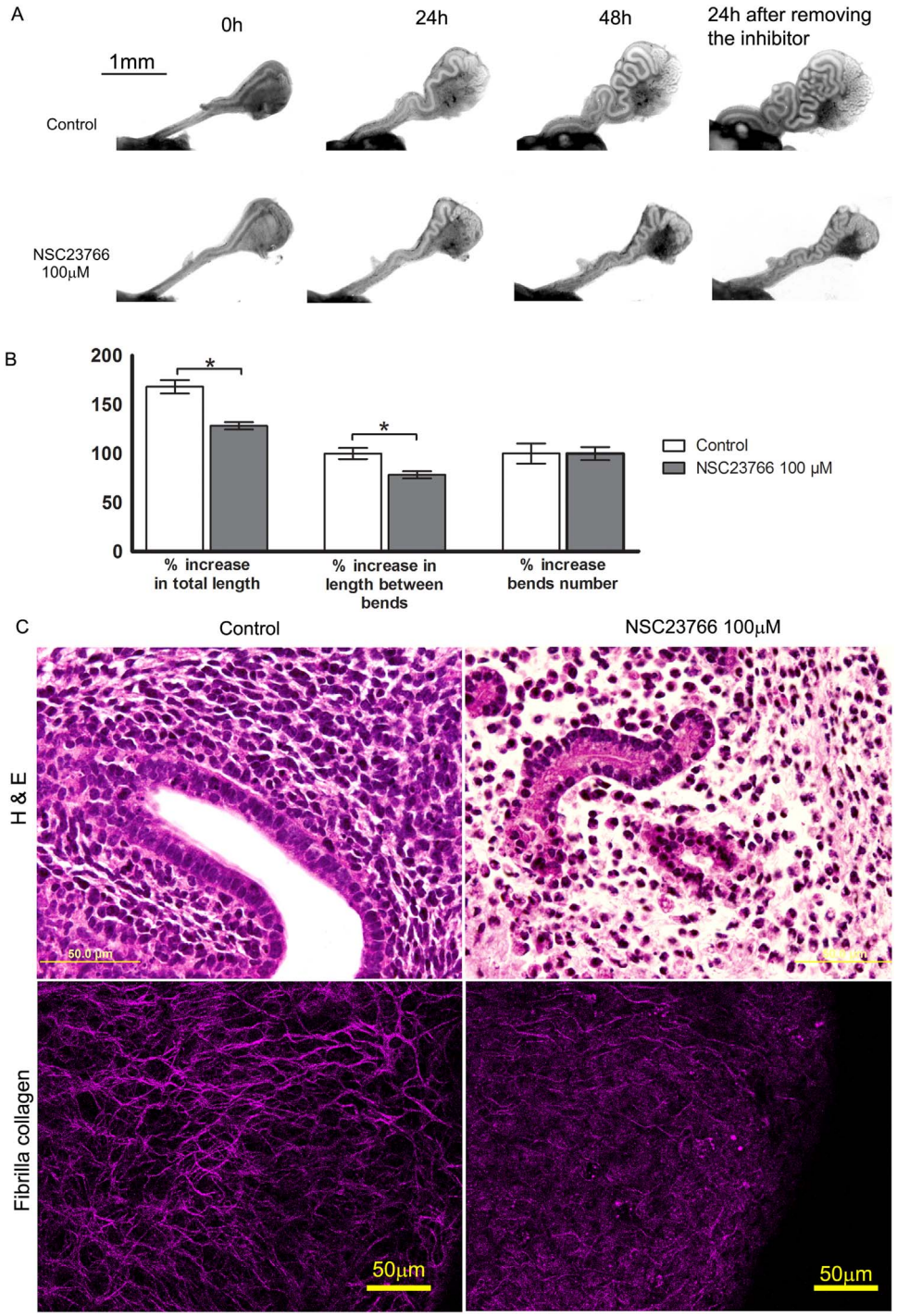

Fig. 6. Effect of RAC1 inhibitor NSC23766 on Wolffian duct morphogenesis. (A) Incubation of Wolffian ducts with 100 μM NSC23766 for 0, 24 and 48 h and also 24 h following inhibitor removal. Note the reduction in elongation in the presence of NSC23766, and elongation was partially rescued upon removal of the inhibitor (from the left, the 4th pair of ducts). (B) Inhibitory effect of NSC23766 on the length and the number of bends of the Wolffian duct during *in vitro* cultures. Data are represented as mean ± SEM, n ≥ 3. (C) Comparison of light images and second harmonic images of control and 24 h NSC23766-treated Wolffian ducts. Note the punctate and loss of organization/assembly of collagen following inhibitor treatment.

deposition and organization of ECM in *Ptk7* TCre-cKOs contributed to the abnormal Wolffian duct phenotype that we observed in these animals. Likely, changes in the ECM integrity resulted in the alteration of Wolffian duct biomechanical properties, which resulted in failure of epithelial cells and mesenchymal cells to undergo mediolateral and radial intercalation respectively, and subsequent failure of the Wolffian duct to undergo elongation and coiling (Fig. 7). However, further studies are needed to examine the mechanisms as to how ECM remodeling changes the biomechanical properties of the ECM, which in turn regulates cell rearrangements and cell movement. We were surprised to observe a decrease in the level of *Npnt* transcripts in cKO epididymides but a high expression of the protein. Upon closer inspection, NPNT was highly disorganized, and presumably, in an abnormal/non-physiological form. Therefore, we hypothesize that the abnormal form would not degrade as rapidly (longer half-life) as the normal form, leading to a loss of function of that protein and contributing to loss of cell movement.

In this study, we used second harmonic generation imaging to

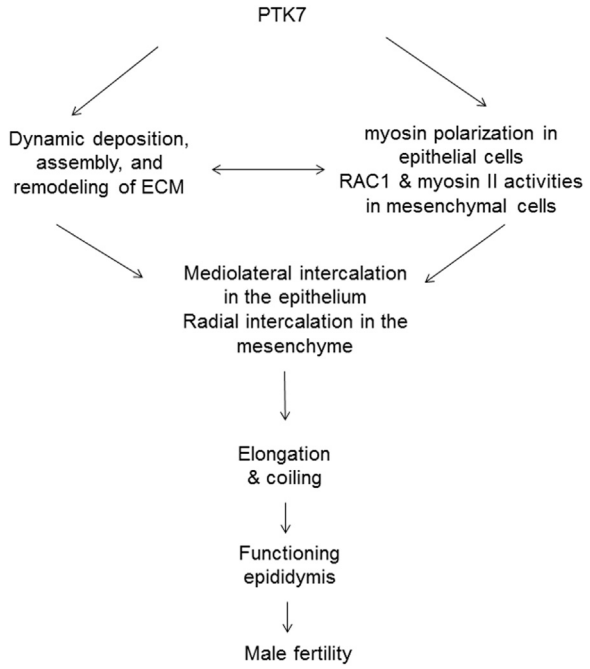

Fig. 7. Overall working hypothesis of the role of PTK7 in the regulation of Wolffian duct morphogenesis. Briefly, PTK7 regulates ECM deposition at the basement membrane and the mesenchyme. PTK7 regulates polarized myosin II activity in epithelial cells and the activities of RAC1 and myosin II in mesenchymal cells. Dynamic remodeling of ECM and intracellular RAC1 and myosin II activities are likely responsible for mediolateral intercalation in the epithelium and radial intercalation in the smooth muscle mesenchyme and *en masse* mesenchymal cell movements within the interstitium. These cell rearrangements and movements are important in Wolffian duct elongation and coiling during morphogenesis, thereby are important in developing a fully functional epididymis that is important for male fertility.

investigate the distribution of fibrilla collagen in the Wolffian duct. When excited by an intense laser light, second harmonic generation takes place in certain mesoscopic structures lacking centrosymmetry such as collagen, myosin, and microtubules (Filova et al., 2010). While procollagen and immature collagen are better visualized using antibody-based immunofluorescence labelling, well organized collagen in the extracellular matrix is better visualized by second harmonic generation imaging (Filova et al., 2010). Application of immunofluorescence and second harmonic generation imaging yielded a whole picture of collagen distribution in the Wolffian duct. The different localization of collagen in Fig. 2 reflected different types and different maturation stages of collagen. PTK7 regulated deposition of immature and fibrilla collagen (Fig. 2). It is recognized that a limitation of our second harmonic generation imaging was that it was not possible to compare fibrils having the same orientation between control and cKO Wolffian ducts. To perform this analysis, we needed to generate a 3D reconstruction of each sample followed by image rotation. Unfortunately, we were not able to perform the analyses because second harmonic imaging requires that intense laser light pass through tissues and care must be taken to avoid tissue damage. We performed Z-stacked imaging but because we needed to avoid a prolonged laser exposure, we did not obtain images of sufficiently high enough resolution to perfrom 3D reconstruction.

3.2. PTK7 regulates myosin II and RAC1 activity

PTK7 is a vertebrate-specific regulator of planar cell polarity (PCP) (Lu et al., 2004). PTK7 regulates neural tube closure, stereociliary bundle orientation, polarized cell motility and convergent extension during gastrulation and neurulation (Lu et al., 2004; Williams et al., 2014). Several studies suggest that PTK7 regulates PCP through regulating myosin II activity (Lee et al., 2012; Williams et al., 2014). In our previous report, we showed that PTK7 regulated polarized myosin II activity in the epithelial cells of the Wolffian duct (Xu et al., 2016). In this study, we showed that PTK7 regulated myosin II activity in SMM cells surrounding the epithelial duct. SMM cells undergo radial intercalation during Wolffian duct morphogenesis. Presumably, PTK7-dependent myosin II activity is involved in the regulation of radial intercalation of mesenchymal cells.

It is unclear how PTK7 signals through RAC1, which is a small GTPase protein in the Rho family and has a central role in regulation of focal adhesions and actin dynamics (Pasapera et al., 2015). Our data showed that RAC1 activity was reduced throughout the mesenchyme following loss of *Ptk7*, suggesting RAC1 was a downstream target of PTK7 signaling. The profound phenotype of *Ptk7* TCre-cKOs may be the result of changes in RAC1 activity, which is a key regulator of cell migration and cell adhesion and regulates many aspects of tissue and organ morphogenesis (Grimsley-Myers et al., 2009). In contrast to a high activity level of RAC1 throughout the mesenchyme, active RAC1 was found at undetectable levels in the Wolffian duct epithelium, suggesting that PTK7/RAC1 signaling was tissue-specific.

RAC1 regulates focal adhesions and actin dynamics, while myosin II is a critical mediator of contractility and focal adhesion dynamics. The interaction between these two signaling molecules is not clear. In migrating cells, RAC1 was thought to locally inhibit non-muscle myosin II activation, and cycles of RAC and RHO activation inactivated and activated non-muscle myosin II, resulting in protrusion and actin bundling, respectively (Vicente-Manzanares et al., 2009). We observed that active RAC1 and active myosin II had opposing activity and localization, likely there were opposing regulatory roles of RAC1 and myosin II during cell rearrangements. However, other studies suggested a different interaction between RAC1 and myosin II signaling. In smooth muscle cells, RAC1 coordinated with RHOA to increase phosphorylation of myosin regulatory light chain, which promoted myosin II activity and cell contraction (Shibata et al., 2015). In the leading edge of migrating cells, RAC1 activation regulated myosin IIA heavy chain phosphorylation that promoted myosin IIA association with focal adhesions and acted as a critical modulator of cell migration and mechanosensing (Pasapera et al., 2015; Shibata et al., 2015). Further studies are required to examine the mechanisms, by which RAC1 and myosin II signaling interact.

3.3. ECM interacts with myosin II and RAC1

We recognize that there is interaction between the remodeling of ECM and myosin II and RAC1 activities, which is shown in the Fig. 7 as double-sided arrows. On one hand, the structure and function of a cell's cytoskeleton is dependent upon the activities of RAC1 and myosin II, and the tension and traction from the cytoskeleton remodel a functional ECM during tissue morphogenesis (Vicente-Manzanares et al., 2009). For example, myosin II drives collagen fiber remodeling (Meshel et al., 2005) and fibronectin fibrillogenesis (Jiang et al., 2003). On the other hand, ECM interacts with cellular receptors such as integrins and receptor tyrosine kinases, and then these cellular receptors transduce ECM signals to the cytoskeleton and nucleus (Bokel and Brown, 2002; Clause and Barker, 2013). Indeed, ECM and cytoskeleton are physically linked through the cellular receptors. The bidirectional flow of information and bidirectional transmission of mechanical forces between the extracellular and intracellular compartments mediate extracellular ECM remodeling and intracellular signal pathways (Clause and Barker, 2013). PTK7 regulates both extracellular ECM remodeling and intracellular signaling and is physically present at the cell membrane, suggesting that it could be one of the links between the extracellular and intracellular compartments.

3.4. ECM and RAC1 activity regulates Wolffian duct morphogenesis

Our *in vitro* experiments provided evidence that a reduction in the degree of collagen crosslinking by collagenase digestion resulted in a decrease in Wolffian duct elongation and coiling and a cyst-like

expansion in the epithelial duct. This finding suggested that integrity of ECM is important for Wolffian duct morphogenesis.

Inhibition of RAC1 activity also resulted in alteration of ECM organization, which was demonstrated by the reduction of fibrilla collagen. More importantly, inhibition of RAC1 activity significantly reduced Wolffian duct elongation, suggesting the importance of RAC activity in the regulation of Wolffian duct morphogenesis.

As summarized in Fig. 7, PTK7 regulates the dynamic remodeling of ECM at the basement membrane and the mesenchyme, and regulates polarized myosin II activity (Xu et al., 2016). In mesenchymal cells, PTK7 regulates the activities of RAC1 and myosin II. Dynamic remodeling of ECM coupled with activities of myosin and RAC1 regulates epithelial cell mediolateral intercalation, mesenchymal cell radial intercalation, and interstitial cell en masse movement. Furthermore, cell intercalation/rearrangement contributes to Wolffian duct elongation and coiling, thereby contributing to developing a fully functional epididymis that is important for male fertility (Fig. 7).

4. Materials and methods

4.1. Animals

Mice were handled according to the approved protocols following the guidelines of the Institutional Animal Care and Use Committee (IACUC) of the University of Virginia. Mice (*Ptk7*$^{flox/flox}$*:mT/mG*) carrying *loxP*-flanked *Ptk7* allele and *mT/mG* (membrane-Tomato/membrane-EGFP) allele mated with mice (*Ptk7*$^{Xst87/+}$*:T-Cre*$^{tg/tg}$) carrying a disrupted allele of *Ptk7* gene, *Xst87* (Lu et al., 2004), and two copies of *T-Cre* to generate conditional knockout (*Ptk7*$^{Xst87/\ flox}$*:T-Cre*^{tg}*: mT/mG*) and control offspring (*Ptk7*$^{+/\ flox}$*:T-Cre*^{tg}*: mT/mG*). *Ptk7* TCre-cKOs and their little mate controls have mixed background of B6C57 and 129. Mice were bred and genotyped based upon the information provided by The Jackson Laboratory (Bar Harbor, Maine).

Wolffian ducts from CD1 wild type mice were used for organ culture since CD1 female mice produce more embryos per pregnancy; an average of 14 embryos per pregnancy, compared to an average of 7 embryos per pregnancy for the B6C57 mice.

4.2. RNAseq sequencing and analysis

The entire epididymis was dissected from the efferent ducts/initial segment junction to the cauda/vas deferens junction from E18.5 control and TCre-cKO embryos. Total RNA was extracted using Qiagen RNeasy Plus Mini Kit (Valencia, CA) according to manufacturer's instructions. Quality control of RNA was conducted using TapeStation and qPCR methods at Genewiz (South Plainfield, NJ). cDNA synthesis and library construction were performed using Illumina Truseq RNASeq (Illumina Inc. San Diego, CA). Four control and four knockout sample replicates were analyzed using an Illumina HiSeq. 2000 instrument at Genewiz (South Plainfield, NJ).

Initial quality assessment of sequencing reads was conducted using FASTQC http://www.bioinformatics.babraham.ac.uk/projects/fastqc/. After aligning data with STAR (Dobin et al., 2013), counted reads were mapped to GENCODE genes using the featureCounts (Liao et al., 2014) software in the Subread package. DESeq. 2 Bioconductor package (Love et al., 2014) in the R statistical computing environment was used to normalize count data and fit to a negative binomial model to assess for differential gene expression between control and TCre-cKO samples. The Benjamini-Hochberg False Discovery Rate (FDR) procedure was used to estimate the adjusted *p*-values for GENCODE/Ensembl gene IDs mapping to known genes. RNAseq data is available in GEO under accession number GSE98715 (https://www.ncbi.nlm.nih.gov/geo/query/acc.cgi?acc=GSE98715). The following secure token has been created to allow review of record GSE98715 while it remains in private status: public when publishing.

To search over-represented or under-represented biological processes, cellular components, molecular functions, and signal pathways, the differentially expressed gene lists generated from RNAseq analysis were submitted to Gene Ontology (www.geneontology.org) and Ingenuity Pathway Analysis (www.ingenuity.com) for enrichment and pathway analyses.

4.3. Wolffian duct organ culture and inhibitor treatment

Embryos from CD1 pregnant female mice were dissected at 15.5 days post-coitum. Wolffian ducts were dissected free of the testes but the efferent ducts and the vas deferens remained. The ducts were cultured on a 0.4 μm Millicell cell culture insert (Millipore, Billerica, MA) in a serum-free DMEM/F12 medium containing 50 μg/ml penicillin streptomycin, 1% ITS (insulin, transferin, and selenium) (Gibco, Langley, OK), and 10^{-8} M testosterone at 37 °C with 5% CO_2 (Xu et al., 2016).

For collagenase IV treatment experiments, E15.5 Wolffian ducts were incubated with DMEM/F12 medium or 0.1 mg/ml collagenase IV for 1, 5, or 10 min and followed with washing in DMEM/F12 medium for 5 times, then cultured on the cell culture insert. Second harmonic generation images were taken at 24 h. Bright field images were taken at 0 h, 24 h, 48 h, and 72 h.

For NSC23766 treatment experiments, Wolffian ducts were incubated with DMSO or 100 μM NSC23766. Second harmonic generation images were taken at 24 h. The bright field images were taken at 0 h, 24 h, and 48 h. After 48 h of culture, NSC23766 was removed, and the images were taken after 24 h of inhibitor withdrawal.

4.4. Immunofluorescence

Wolffian duct tissue samples were immersion-fixed in 4% paraformaldehyde (PFA) in PBS (phosphate buffered saline) overnight at 4 °C followed by paraffin embedding and sectioning. Knockout and control sections were placed on the same slide side by side to ensure similar treatment. Subsequently, slides were deparaffinized and rehydrated. For antigen retrieval, slides were microwaved in antigen unmasking solution (Vector Laboratories, Burlingame, CA) for 10 min on high in a 1300 W microwave and cooled for 1 h at room temperature. Following blocking in blocking solution with 10% (v/v) normal goat or donkey serum (Vector Laboratories, Burlingame, CA), 0.5% (v/v) gelatin from cold-water fish skin (Sigma, St. Louis, MO), and TBS (tris-buffered saline) for 1.5 h, slides were incubated overnight at 4 °C in blocking solution with the primary antibodies. Following washing in TBS, slides were incubated with 1:250 dilution of Alexa Fluor 594 secondary antibodies (Molecular Probe, Eugene, OR) in blocking solution for 1.5 h at room temperature. All slides were washed in TBS and mounted using Prolong Anti-fade reagent with DAPI for nuclear staining (Molecular Probe, Eugene, OR) and viewed under a Zeiss microscope equipped with epifluorescence. COL4 (collagen, type IV) antibody (#AB769, 1:200 working dilution) was purchased from Millipore (Billerica, MA).

4.5. Whole mount immunofluorescence and confocal and two-photon-imaging

E18.5 to P1 Wolffian ducts were fixed in 4% PFA at 4 °C for 1–3 h prior to washes in PBS at room temperature and permeabilized in tsPBS (0.5% Triton X-100 and 0.1% saponin in PBS) at 4 °C overnight on a rocker. Samples were then incubated in a blocking solution (10% normal goat serum in tsPBS) for 1 h at room temperature and then incubated overnight at 4 °C in blocking solution with the primary antibodies. Following washing in tsPBS, slides were incubated with 1:200 dilution of Alexa Fluor 594 secondary antibodies (Molecular Probe, Eugene, OR) in blocking solution overnight at 4 °C. All samples were post-fixed in 4% PFA at 4 °C for 0.5 h and then washed and stored

in PBS before imaging. Samples were then incubated in Sca/eA2 solution (4 M urea, 10% glycerol, and 0.1% Triton X-100) (Hama et al., 2011) for at least 0.5 h before visualizing under a Zeiss 780 confocal microscope. Primary antibodies included phospho-RLC antibody (#31694, 1:100 working dilution) from Rockland (Limerick, PA); Laminin antibody (#L9393, 1:200 working dilution) from Sigma-Aldrich (St. Louis, MO); COL4 (collagen, type IV) antibody (#AB769, 1:200 working dilution) from Millipore (Billerica, MA); Active RAC1-GTP antibody (#26903, 1:400 working dilution) from NewEast Biosciences (King of Prussia, PA); NPNT antibody is gifted from Dr. Hironobu Fujiwara (RIKEN Center for Developmental Biology, Kobe, Japan) (Linton et al., 2007).

The images from a certain focal plane were referred as to co-focal images. Three dimensional reconstruction of a stack of images were generated using Volocity 6.3 software (PerkinElmer,Waltham, MA).

Extracellularly distributed collagen was visualized by joint application of two-photon excitation microscopy and second-harmonic generation imaging using 860 nm excitation wavelength and 430 nm emission wavelength (Filova et al., 2010).

To ensure similar treatment, the labelling processes of control and TCre-cKO Wolffian ducts were conducted in the same well. The images for controls and knockouts were taken from the identical Wolffian duct region and using identical imaging parameters. At least three Wolffian ducts were observed for each group.

4.6. Statistics

One way analysis-of-variance (ANOVA) was performed to identify significant differences of means. Significant differences were indicated by *($p < 0.05$), ** ($p < 0.01$), and ***($p < 0.001$).

Acknowledgments

We thank Angela Washington for her assistance in performing experiments and Dr. Zuzana Burdíková for her advice on second harmonic generation imaging. We thank Dr. Mark Lewandoski at National Cancer Institute for the T-Cre mouse line. We acknowledge the Keck Center for Cellular Imaging for the usage of the Zeiss 780 confocal/multiphoton microscopy system (OD016446).

Funding

This work was supported by Eunice Shriver National Institute of Child Health and Human Development/NIH [grant number RO1-HD069654].

References

Bokel, C., Brown, N.H., 2002. Integrins in development: moving on, responding to, and sticking to the extracellular matrix. Dev. Cell 3, 311–321.
Bonnans, C., Chou, J., Werb, Z., 2014. Remodelling the extracellular matrix in development and disease. Nat. Rev. Mol. Cell Biol. 15, 786–801.
Clause, K.C., Barker, T.H., 2013. Extracellular matrix signaling in morphogenesis and repair. Curr. Opin. Biotechnol. 24, 830–833.
Dobin, A., Davis, C.A., Schlesinger, F., Drenkow, J., Zaleski, C., Jha, S., Batut, P., Chaisson, M., Gingeras, T.R., 2013. STAR: ultrafast universal RNA-seq aligner. Bioinformatics 29, 15–21.
Filova, E., Burdikova, Z., Rampichova, M., Bianchini, P., Capek, M., Kostakova, E., Amler, E., Kubinova, L., 2010. Analysis and three-dimensional visualization of collagen in artificial scaffolds using nonlinear microscopy techniques. J. Biomed. Opt. 15, 066011.
Girgis, S.M., Etriby, A.N., Ibraim, A.A., Kahil, S.A., 1969. Testicular biopsy in azoospermia. A review of the last ten years' experiences of over 800 cases. Fertil. Steril. 20, 467–477.
Grimsley-Myers, C.M., Sipe, C.W., Geleoc, G.S., Lu, X., 2009. The small GTPase Rac1 regulates auditory hair cell morphogenesis. J. Neurosci.: Off. J. Soc. Neurosci. 29, 15859–15869.
Hama, H., Kurokawa, H., Kawano, H., Ando, R., Shimogori, T., Noda, H., Fukami, K., Sakaue-Sawano, A., Miyawaki, A., 2011. Scale: a chemical approach for fluorescence imaging and reconstruction of transparent mouse brain. Nat. Neurosci. 14, 1481–1488.
Hinton, B.T., Galdamez, M.M., Sutherland, A., Bomgardner, D., Xu, B., Abdel-Fattah, R., Yang, L., 2011. How do you get six meters of epididymis inside a human scrotum? J. Androl. 32, 558–564.
Jiang, G., Giannone, G., Critchley, D.R., Fukumoto, E., Sheetz, M.P., 2003. Two-piconewton slip bond between fibronectin and the cytoskeleton depends on talin. Nature 424, 334–337.
Joseph, A., Yao, H., Hinton, B.T., 2009. Development and morphogenesis of the Wolffian/epididymal duct, more twists and turns. Dev. Biol. 325, 6–14.
Kroovand, R., Perlmutter, A., 1981. Pediatric Andrology. Martinus Nijhoff Publishers, Boston.
Lee, J., Andreeva, A., Sipe, C.W., Liu, L., Cheng, A., Lu, X., 2012. PTK7 regulates myosin II activity to orient planar polarity in the mammalian auditory epithelium. Curr. Biol.: CB 22, 956–966.
Liao, Y., Smyth, G.K., Shi, W., 2014. featureCounts: an efficient general purpose program for assigning sequence reads to genomic features. Bioinformatics 30, 923–930.
Linton, J.M., Martin, G.R., Reichardt, L.F., 2007. The ECM protein nephronectin promotes kidney development via integrin alpha8beta1-mediated stimulation of Gdnf expression. Development 134, 2501–2509.
Love, M.I., Huber, W., Anders, S., 2014. Moderated estimation of fold change and dispersion for RNA-seq data with DESeq. 2. Genome Biol. 15, 550.
Lu, X., Borchers, A.G., Jolicoeur, C., Rayburn, H., Baker, J.C., Tessier-Lavigne, M., 2004. PTK7/CCK-4 is a novel regulator of planar cell polarity in vertebrates. Nature 430, 93–98.
Meshel, A.S., Wei, Q., Adelstein, R.S., Sheetz, M.P., 2005. Basic mechanism of three-dimensional collagen fibre transport by fibroblasts. Nat. Cell Biol. 7, 157–164.
Pasapera, A.M., Plotnikov, S.V., Fischer, R.S., Case, L.B., Egelhoff, T.T., Waterman, C.M., 2015. Rac1-dependent phosphorylation and focal adhesion recruitment of myosin IIA regulates migration and mechanosensing. Curr. Biol.: CB 25, 175–186.
Perantoni, A.O., Timofeeva, O., Naillat, F., Richman, C., Pajni-Underwood, S., Wilson, C., Vainio, S., Dove, L.F., Lewandoski, M., 2005. Inactivation of FGF8 in early mesoderm reveals an essential role in kidney development. Development 132, 3859–3871.
Shibata, K., Sakai, H., Huang, Q., Kamata, H., Chiba, Y., Misawa, M., Ikebe, R., Ikebe, M., 2015. Rac1 regulates myosin II phosphorylation through regulation of myosin light chain phosphatase. J. Cell. Physiol. 230, 1352–1364.
Sit, S.T., Manser, E., 2011. Rho GTPases and their role in organizing the actin cytoskeleton. J. Cell Sci. 124, 679–683.
Snyder, E.M., Small, C.L., Bomgardner, D., Xu, B., Evanoff, R., Griswold, M.D., Hinton, B.T., 2010. Gene expression in the efferent ducts, epididymis, and vas deferens during embryonic development of the mouse. Dev. Dyn.: Off. Publ. Am. Assoc. Anat. 239, 2479–2491.
Turek, P.J., Ewalt, D.H., Snyder, H.M., Duckett, J.W., 1994. Normal epididymal anatomy in boys. J. Urol. 151, 726–727.
Vicente-Manzanares, M., Ma, X., Adelstein, R.S., Horwitz, A.R., 2009. Non-muscle myosin II takes centre stage in cell adhesion and migration. Nat. Rev. Mol. Cell Biol. 10, 778–790.
Walck-Shannon, E., Hardin, J., 2014. Cell intercalation from top to bottom. Nat. Rev. Mol. Cell Biol. 15, 34–48.
Williams, M., Yen, W., Lu, X., Sutherland, A., 2014. Distinct apical and basolateral mechanisms drive planar cell polarity-dependent convergent extension of the mouse neural plate. Dev. Cell 29, 34–46.
Xu, B., Washington, A.M., Domeniconi, R.F., Ferreira Souza, A.C., Lu, X., Sutherland, A., Hinton, B.T., 2016. Protein tyrosine kinase 7 is essential for tubular morphogenesis of the Wolffian duct. Dev. Biol. 412, 219–233.